

# Effects of the Vibrational and Rotational Energy on Reaction Cross-Section in a Classical Trajectory Study of Atom-Diatomic Molecule Collisions

Hamzeh M. Abdel-Halim and Sawsan M. Jaafreh

The Hashemite University, Faculty of Science, Department of Chemistry, P.O. Box 330127, Zarqa 13133, Jordan

Reprint requests to Dr. H. M. A.-H.; E-mail: hamzehah@hu.edu.jo

Z. Naturforsch. **63a**, 721 – 734 (2008); received April 17, 2008

Effects of the initial vibrational and rotational energy of a diatomic molecule on reaction rates of atom-diatomic molecule reactions have been studied using classical trajectory calculations. The reaction probabilities, cross-sections and rate constants were calculated using the three-dimensional Monte-Carlo method. Equations of motion, which predict the positions and momenta of the colliding particles after each step in the trajectory, have been integrated numerically by the Runge-Kutta-Gill and Adams-Moulton methods. Morse potential energy surfaces were used to describe the interaction between the atom and each atom in the diatomic molecule. Several atom-diatomic molecule systems were studied. Variation of the reaction cross-section with both vibrational and rotational quantum numbers has been studied. For all systems studied, it was found that the cross-section increases with the vibrational quantum number. However, the effect of rotational quantum number on cross-section varies from one system to another.

Results obtained in the present work were compared with experimental data and/or with results obtained theoretically. Good agreements were observed with experimental and with theoretical results obtained by other investigators using different calculation methods.

*Key words:* Cross-Section; Vibration; Rotation; Atom-Diatom; Classical Trajectories.

## 1. Introduction

The internal energy of a molecule plays an important role in determining its physical and chemical properties. The reaction probability of a diatomic molecule with an atom depends on the “ease” of bond breaking and bond formation. This depends on the collision energy of the colliding particles and also depends on the bond strength of the diatomic molecule. For a specific diatomic molecule, its bond strength, and hence the probability of bond breaking, depends on both its vibrational and rotational states.

For reactive collisions between an atom (A) and a diatomic molecule (BC), the process is simplified by bond breaking of BC and bond formation of AB or AC. Such collisions can be studied using quantum, classical or semi-classical mechanical methods. The quantum mechanical solution is done by solving the Schrödinger equation;  $\hat{H}\Psi = E\Psi$ , where  $\hat{H}$  is the Hamiltonian operator,  $\Psi$  the wave function and  $E$  the energy. Solving this equation is difficult because an exact wave function for the system is hard to find. On the

other hand, classical methods of calculations are easier to carry out, and they are well established. The classical solution involves classical trajectories by solving Hamilton's equations of motion in order to determine the position and the momentum of each of the colliding particles in every step of the trajectory during the collision. In the present work, a semi-classical method was employed, in which classical trajectories, involving the use of quantum mechanical parameters, were used in the calculations. The classical trajectories method has been widely used to study reactive collisions between atoms and diatomic molecules [1 – 15]. It provides a reliable method for the calculation of the reaction probability, from which the reaction cross-section and rate constant can be calculated. This method is frequently used to compare theoretical with experimental results.

The effect of the collision energy on reaction rates, which is determined by the translational energy of the system, had been studied by the authors [1]. Using a different method and/or different potential energy surfaces to describe interactions between colliding particles, the effect of vibrational and/or rotational states of

the diatomic molecule had been studied by several investigators. Porter et al. [2] used a quasi-classical procedure for the examination of the collision dynamics of the  $\text{H} + \text{H}_2$  reaction by means of Monte Carlo averages over a large number of classical trajectories. The total reaction cross-section was determined as a function of initial relative velocity and the initial molecular vibrational-rotational state. Persky [3] reported the rate constants, isotope effects, and energy disposal features for the  $\text{Cl} + \text{HD}$  reaction. Using their own ab initio potential energy surface, Schinke and Lester [4] reported rate constant calculations for the reaction of  $\text{O}(^3\text{P})$  with  $\text{H}_2$ . Their calculations were in good agreement with the experimental rate constant at 302 K. Zuhrt et al. [5] used quasi-classical trajectory (QCT) calculations for the reaction of  $\text{He} + \text{H}_2^+$ . They studied the effect of reactants' translational, vibrational, and rotational energies on reaction cross-sections. Their results showed that a higher vibrational energy of the diatomic molecule is more effective in promoting the reaction than the translational energy. Weisshaar et al. [6] reported experimental rate constants for the proton transfer reactions  $\text{F}^- + \text{HX} \rightarrow \text{HF}(v) + \text{X}^-$ ,  $\text{X} = \text{Cl}, \text{Br},$  and  $\text{I}$ . Phillips et al. [7] reported results of state-to-state dynamics experiments of the  $\text{D} + \text{H}_2 \rightarrow \text{HD} + \text{H}$  reaction. Product state distributions and absolute partial cross-sections had been determined using anti-Stokes-Raman scattering spectra of HD. Classical trajectory calculations for the reaction  $\text{D} + \text{H}_2(v=0, j=0-3) \rightarrow \text{HD}(v', j') + \text{H}$  had been performed by Aoiz et al. [8]. Differential and state-to-state reaction cross-sections were calculated in the 0.35–1.10 eV collision energy range. The effect of translational, rotational, and vibrational energy on the dynamics of  $\text{D} + \text{H}_2$  using classical trajectory calculations had been studied by Aoiz et al. [9]. Quasi-classical trajectory calculations for the  $\text{D} + \text{H}_2(v, j) \rightarrow \text{HD} + \text{H}$  system had been performed on an LSTH potential energy surface in order to study the combined effects of translation, rotation, and vibration on reactivity. Meilke et al. [10] reported reaction probabilities for the reaction  $\text{Br} + \text{H}_2(v, j) \rightarrow \text{H} + \text{HBr}$  and  $\text{Br}^* + \text{H}_2(v, j) \rightarrow \text{H} + \text{HBr}$ . They studied the competition between an electronically nonadiabatic reaction and electronic-to-vibrational, rotational, and translational energy transfer in the reaction of  $\text{Br}^*$  with  $\text{H}_2$ . Moribayashi and Nakamura [11] studied the hydrogen atom transfer reaction between two heavy atoms;  $\text{O} + \text{HCl} \rightarrow \text{OH} + \text{Cl}$ . The system was studied quantum-mechanically accurately with the use of the hyperspherical coordinate approach,

taking into account several vibrational and several rotational states of the HCl molecule. McCaffery et al. [12] introduced a quantum-constrained kinematic model for atom-diatom reactive collisions. Their approach emphasized the disposal of the initial relative momentum into the rotational angular momentum of the diatomic product via vector relations that are constrained by the internal quantum structure of the product. Lee and Farrar [13] studied the vibrational state of the  $\text{O}^- + \text{H}_2$  reaction and the effects of isotopes on the product energy partitioning. Quantitative calculations of the product rovibrational (rotational and vibrational) distribution from atom-diatom exchange reactions had been performed by Marsh et al. [14]. The basis of their model is a momentum interconversion at a critical configuration defined in terms of molecular dimensions of the species involved. They claimed that good agreement is obtained between the experimental and calculated  $(v, j)$  distribution for a wide range of elementary reactions. Miller [15] reported a method of semi-classical initial value representation which provides a potentially practical way for adding quantum mechanical effects to classical molecular dynamics simulations of the dynamics of complex molecular systems that have many degrees of freedom. The method was found to be useful in many applications such as photodissociation, photodetachment spectra, electronic nuclear problems, inelastic scattering, and spectral densities.

In the present work, the reaction probabilities for several atom-diatomic molecule reactions are calculated using a Monte Carlo classical trajectory method. Morse potential energy surfaces are applied for the interactions between the atom and the diatomic molecule. The probability of the reaction, the reaction cross-section and the rate constant are calculated at various initial values of the dynamical variables. Calculations are performed for each atom-diatom system at various vibrational and various rotational states. Effects of the initial vibrational state and the initial rotational state of the molecule on the reaction probability are presented. The calculated values are compared with the available experimental values to check the validity and the accuracy of the method. All calculations are performed using a FORTRAN compiler from Salford University.

## 2. Method of Calculations

The details of the method of calculation are mentioned in our previous publication [1]. The use of the

classical trajectory method to calculate reaction probabilities involves solving numerically Hamilton's equations of motion for the collision particles. Hamilton's equations are described by the general dynamics  $Q_j$  and  $P_j$ , given by

$$\begin{aligned} \frac{dQ_j}{dt} &= \dot{Q}_j = \frac{\partial H'}{\partial P_j} = \frac{\partial T}{\partial P_j}, \\ \frac{dP_j}{dt} &= \dot{P}_j = -\frac{\partial H'}{\partial Q_j} = -\frac{\partial V}{\partial Q_j}, \end{aligned} \quad (1)$$

where  $H'$  is the classical Hamiltonian that equals to the sum of kinetic energy operator,  $T$ , and the potential energy operator,  $V$ . The numerical integration solution of Hamilton's equations determines the position,  $Q_j$ , and the momentum,  $P_j$ , for each particle as a function of time during the pathway of the trajectory.

For the interatomic separations: A – B( $R_1$ ), B – C( $R_2$ ), and A – C( $R_3$ ), the Hamiltonian function for a potential  $V(R_1, R_2, R_3)$  has the form

$$H' = \frac{1}{2\mu_{BC}} \sum_{j=1}^3 P_j^2 + \frac{1}{2\mu_{A,BC}} \sum_{j=4}^6 P_j^2 + V(R_1, R_2, R_3), \quad (2)$$

where  $\mu_{BC}$  is the reduced mass of atoms B and C and  $\mu_{A,BC}$  is the reduced mass for atom A and the molecule BC. Here, there are 12 simultaneous differential equations to be integrated for the determination of the time variation of  $Q_j$  and  $P_j$ .

### 2.1. Initial Values of the Dynamical Variables

The initial state of a trajectory is defined by specifying values for the dynamical variables. Dynamical variables include the orientation angles, impact parameter, initial separation of the colliding particles, and the initial relative velocity. Some simplifications on the initial state of the system were introduced. The  $z$ -axis was chosen as the direction of the initial relative velocity of atom A towards the BC molecule ( $v_{rel}$ ), thus  $v_{rel} = v_z$  and  $v_x = v_y = 0$ . The orientation of atom A and the centre of mass of BC was chosen to be in the  $yz$ -plane. The angles that define the orientation of BC in the three-atom polar coordinate system and the impact parameter, which is the distance of closest approach of A from the centre of mass of BC, were selected randomly by Monte Carlo techniques [9]. The

values of the other parameters were assigned arbitrarily. The initial distance between atom A and the centre of mass of BC was chosen such that the interaction of A with BC is negligible. The two classical turning-points of the diatom were selected alternatively to be the initial values of the internuclear separation of the molecule BC. The initial rotational and vibrational energies for the diatomic molecule were calculated from the assigned rotational and vibrational quantum number values [1]. Other spectroscopic constants for molecules AB, BC, and AC were taken from the literature [16–18].

### 2.2. Potential Energy Surfaces

In the present work, Morse potential energy surfaces are used to describe the interaction between atoms involved in the collision process; they are given by

$$\begin{aligned} V_{AB} &= D_1[1 - \exp\{-\alpha_1(R_1 - Re_1)\}]^2 - D_1, \\ V_{BC} &= D_2[1 - \exp\{-\alpha_2(R_2 - Re_2)\}]^2 - D_2, \quad (3) \\ V_{AC} &= D_3[1 - \exp\{-\alpha_3(R_3 - Re_3)\}]^2 - D_3, \end{aligned}$$

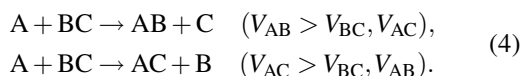
where  $V_{AB}$ ,  $V_{BC}$  and  $V_{AC}$  are the potentials between atom pairs (A – B), (B – C), and (A – C), respectively. The parameters  $R_1$ ,  $R_2$  and  $R_3$ , as defined before, represent the inter-atomic separations for the molecules AB, BC, and AC, respectively. The constants  $D_j$ ,  $\alpha_j$ , and  $Re_j$  ( $j = 1, 2, 3$ ) are the spectroscopic constants for AB, BC, and AC molecules, respectively.

After specifying the initial values of the dynamical variables and choosing the potential energy surfaces between interacting atoms, the classical trajectory can be started. Hamilton's equations of motions were integrated numerically by the Runge-Kutta-Gill (RKG) fourth-order method and the Adams-Molton (AM) [19] corrector and predictor method. To reduce computer time, the first five cycles of each trajectory were done by the RKG method, then the integration was shifted to a higher gear using the AM method. The integration interval size used was chosen between  $2.15 \cdot 10^{-15}$  and  $2.15 \cdot 10^{-16}$  s. The accuracy of the numerical integration was checked by the following methods: First, by the constancy of the total energy throughout the trajectory, which serves as a crude test for the integration accuracy for a nonreactive collision. Second, by the back-integration method, in which the direction of the momenta at the end of the trajectory is reversed and then integrated back to the initial state. Third,

by comparing results of several trajectories that have the same initial states but different integration interval sizes.

### 2.3. End of Trajectory: Reaction Probability, Cross-Section and Rate Constant

As the trajectory proceeds, atom A starts moving in steps towards the BC molecule. After each step, new positions and new momenta for each particle are determined by the numerical integration. When the distance of A from the centre of mass of BC reaches a minimum, the interaction of A with both B and C is maximal and hence the reaction probability is maximal. Depending on whether a reaction occurs or not, an atom (A, B, C) starts moving away from the molecule (BC, AC, AB) until it reaches a distance where its interaction with both atoms of the molecule is negligible. At this distance the trajectory is ended. At the end of the trajectory, the potential values between atomic pairs,  $V_{AB}$ ,  $V_{BC}$ , and  $V_{AC}$ , determine whether a reaction occurs or not. If  $V_{BC}$  is greater than both  $V_{AB}$  and  $V_{AC}$ , no reaction occurs. In this case, atom A collides and then flies away from the BC molecule. Here, exchange of energy between A and BC may or may not occur, depending on whether the collision is inelastic or elastic, respectively. On the other hand, if  $V_{AB}$  is greater than both  $V_{BC}$  and  $V_{AC}$ , then a reaction occurs and an AB molecule is produced. However, if  $V_{AC}$  is the greatest, the molecule AC forms. The possible reactions are:



The corresponding probabilities at a given temperature  $T$ ,  $P(T)$ , are given by

$$P_{AB,AC}(T) = \frac{\text{number of AB or AC produced}}{\text{total number of trajectories}}. \quad (5)$$

The reaction cross-section,  $\sigma_r$ , is related to  $P(T)$  and the collision cross-section,  $\sigma$ , by the relation [20]

$$\sigma_r = P(T)\sigma. \quad (6)$$

The rate constant for the reaction is given by [20]

$$k(T) = \bar{v}_{rel}\sigma_r e^{-E_0/k_B T}, \quad (7)$$

where  $\bar{v}_{rel}$  is the average relative velocity and  $E_0$  is the barrier energy for the reaction.

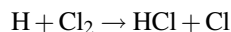
## 3. Results and Discussion

To mimic the experimental situation, a large number of trajectories were performed for each reactive collision studied. Depending on the reaction temperature, step size of integration selected, and other initial parameters, the number of trajectories performed was between 10,000–60,000 trajectories. The maximum number of trajectories is chosen when there is no *significant* change in the results produced (less than 2.00%). Only “good trajectories” were included in the calculations. A “good trajectory” is one that *passes* accuracy check and has less than 1.00% errors. Considering this, and considering other sources of errors mentioned earlier, we believe that our reported rate constants have less than 3.00% errors. Each trajectory is unique by the set of its initial values of the dynamical variables, which were chosen randomly. For each system studied, calculations were performed at three vibrational quantum numbers ( $v = 0, 1, 2$ ). Within each vibrational level, several rotational quantum numbers  $J$  were selected. Values of selected  $J$ 's were chosen to include the rotational level of the molecule with maximal populations  $J_{max}$  at a selected temperature. Unless otherwise stated, the reactions were studied at 300 K. The calculated reaction probabilities, cross-sections, and rate constants for some selected systems are shown in Tables 1–20. Variation of the reaction cross-section and rate constant are shown in Figs. 1–17. Comparison with experimental and/or with other theoretical values obtained at the same conditions have been made.

Looking physically at the reaction processes that may happen due to a collision of an atom with a diatomic molecule, the reaction will occur if enough translational energy from the atom is transferred to the molecule to cause its bond to break. The probability of a reaction to happen depends on several factors; for example, it depends on the collision energy of the colliding particles, which depends on the collision temperature and orientation of the collision, and on the bond strength of the diatomic molecule. In the present study, the collision temperature was kept constant at 300 K. Regarding the collision orientation, all possible orientations have been considered in the calculations using random number generator software. For a specific molecule, its bond strength depends on the electronic, vibrational and rotational states of the molecule. At the calculation conditions, 300 K, almost all molecules are in the ground electronic state. However, several

vibrational and rotational states are available for the molecule, which accordingly, leads to variation in the bond strength of the molecule. Therefore, one would expect variations in the reaction probability as the vibrational and/or rotational state of the molecule varies; this is what we will study in the present work. Previous calculations [21], done in our laboratory, on the energy transfer in atom-diatomic molecule collisions showed that the translational to vibrational energy transfer increases as the vibrational quantum number of the molecule increases. This leads to a weakening of the bond, and hence, to higher reaction probability. Within the same vibrational state and for various rotational quantum numbers, the amount of energy transfer from translational to vibrational and rotational energies varies with the nature of the diatomic molecule, i. e. its reduced mass, well depth, and its potential well width. Therefore, no general trend of the dependence of the reaction probability on the rotational quantum number of the molecule can be identified, and each system will be treated separately. Several colliding particles were chosen, taking into consideration the masses, well depths and widths. Below, are details for each reaction studied.

### 3.1. Reactions of Hydrogen Atoms with Chlorine Molecules



The reaction probabilities and reactions cross-sections for this reaction were calculated at various  $v$  and  $J$  values. The results are shown in Table 1. The calculated reaction rate constants are shown in

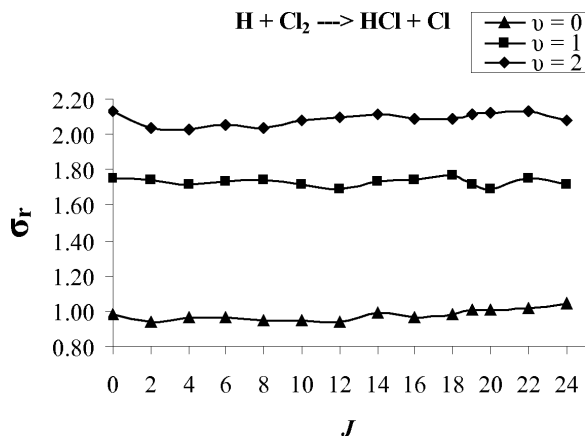


Fig. 1. Variation of the reaction cross-section  $\sigma_r$  for the reaction  $\text{H} + \text{Cl}_2 \rightarrow \text{HCl} + \text{Cl}$  with both  $v$  and  $J$  values.

Table 1. Calculated probabilities  $[P(T)]$  and reaction cross-sections ( $\sigma_r$ ), in  $\text{\AA}^2$ , for the reaction  $\text{H} + \text{Cl}_2 \rightarrow \text{HCl} + \text{Cl}$  at various  $v$  and  $J$  values.

$J$	$v=0$		$v=1$		$v=2$	
	$P(T)$	$\sigma_r$	$P(T)$	$\sigma_r$	$P(T)$	$\sigma_r$
0	0.0563	0.983	0.100	1.75	0.122	2.13
2	0.0537	0.938	0.0998	1.74	0.117	2.04
4	0.0551	0.963	0.0982	1.72	0.116	2.03
6	0.0550	0.961	0.0993	1.73	0.118	2.05
8	0.0543	0.949	0.0996	1.74	0.117	2.04
10	0.0542	0.947	0.0984	1.72	0.119	2.08
12	0.0535	0.935	0.0969	1.69	0.120	2.10
14	0.0568	0.992	0.0992	1.73	0.121	2.11
16	0.0554	0.967	0.0997	1.74	0.120	2.09
18	0.0560	0.978	0.101	1.77	0.120	2.09
19	0.0580	1.01	0.0987	1.72	0.121	2.11
20	0.0578	1.01	0.0969	1.69	0.121	2.12
22	0.0582	1.02	0.100	1.75	0.122	2.13
24	0.0596	1.04	0.0983	1.72	0.119	2.08

Table 2. Calculated reaction rate constants  $[k(T)]$  for the reaction  $\text{H} + \text{Cl}_2 \rightarrow \text{HCl} + \text{Cl}$  at various  $v$  and  $J$  values.

$J$	$k(T)$ [ $\text{cm}^3 \text{ molecule}^{-1} \text{ s}^{-1}$ ]		
	$v=0$	$v=1$	$v=2$
0	$2.48 \cdot 10^{-11}$	$4.41 \cdot 10^{-11}$	$5.36 \cdot 10^{-11}$
2	$2.36 \cdot 10^{-11}$	$4.39 \cdot 10^{-11}$	$5.14 \cdot 10^{-11}$
4	$2.43 \cdot 10^{-11}$	$4.32 \cdot 10^{-11}$	$5.12 \cdot 10^{-11}$
6	$2.42 \cdot 10^{-11}$	$4.37 \cdot 10^{-11}$	$5.17 \cdot 10^{-11}$
8	$2.39 \cdot 10^{-11}$	$4.38 \cdot 10^{-11}$	$5.14 \cdot 10^{-11}$
10	$2.39 \cdot 10^{-11}$	$4.33 \cdot 10^{-11}$	$5.25 \cdot 10^{-11}$
12	$2.36 \cdot 10^{-11}$	$4.27 \cdot 10^{-11}$	$5.30 \cdot 10^{-11}$
14	$2.50 \cdot 10^{-11}$	$4.37 \cdot 10^{-11}$	$5.32 \cdot 10^{-11}$
16	$2.44 \cdot 10^{-11}$	$4.39 \cdot 10^{-11}$	$5.26 \cdot 10^{-11}$
18	$2.46 \cdot 10^{-11}$	$4.46 \cdot 10^{-11}$	$5.26 \cdot 10^{-11}$
19	$2.55 \cdot 10^{-11}$	$4.34 \cdot 10^{-11}$	$5.32 \cdot 10^{-11}$
20	$2.55 \cdot 10^{-11}$	$4.27 \cdot 10^{-11}$	$5.34 \cdot 10^{-11}$
22	$2.56 \cdot 10^{-11}$	$4.42 \cdot 10^{-11}$	$5.37 \cdot 10^{-11}$
24	$2.62 \cdot 10^{-11}$	$4.33 \cdot 10^{-11}$	$5.25 \cdot 10^{-11}$

Table 2. Variations of the reaction cross-section with both  $v$  and  $J$  values are shown in Figure 1. The results show that the reaction probability (as well as the cross-section and rate constant) increases as the vibrational quantum number increases. This is an expected result. As the molecule goes to a higher vibrational state, its bond weakens. This increases the probability of breaking the bond and also the probability of HCl formation. However, the results show minor changes in the rate constant with varying the  $J$  values. For a relatively large molecule like  $\text{Cl}_2$ , increasing the rotational energy has a smaller effect on its bond strength and hence little effect on the probability of HCl formation. Comparing (at 300 K, at which  $v=0$  and  $J=J_{\text{max}}$ ) our calculated rate constant of  $2.55 \cdot 10^{-11} \text{ cm}^3 \text{ molecule}^{-1} \text{ s}^{-1}$  with the experimental

Table 3. Calculated probabilities [ $P(T)$ ] and reaction cross-sections ( $\sigma_r$ ), in  $\text{\AA}^2$ , for the reaction  $\text{Cl} + \text{H}_2 \rightarrow \text{HCl} + \text{H}$  at various  $v$  and  $J$  values.

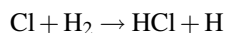
$J$	$v = 0$		$v = 1$		$v = 2$	
	$P(T)$	$\sigma_r$	$P(T)$	$\sigma_r$	$P(T)$	$\sigma_r$
0	0.0805	0.758	0.362	3.41	0.510	4.80
1	0.0782	0.737	0.236	2.23	0.379	3.57
2	0.0779	0.734	0.0844	0.795	0.0882	0.831
3	0.0786	0.741	0.0849	0.800	0.0830	0.782
4	0.0783	0.738	0.0815	0.767	0.0847	0.798
5	0.0785	0.739	0.0810	0.763	0.0814	0.767

Table 4. Calculated reaction rate constants [ $k(T)$ ] for the reaction  $\text{Cl} + \text{H}_2 \rightarrow \text{HCl} + \text{H}$  at various  $v$  and  $J$  values.

$J$	$k(T)$ [ $\text{cm}^3 \text{molecule}^{-1} \text{s}^{-1}$ ]		
	$v = 0$	$v = 1$	$v = 2$
0	$1.84 \cdot 10^{-14}$	$8.28 \cdot 10^{-14}$	$1.17 \cdot 10^{-13}$
1	$1.79 \cdot 10^{-14}$	$5.41 \cdot 10^{-14}$	$8.67 \cdot 10^{-14}$
2	$1.78 \cdot 10^{-14}$	$1.93 \cdot 10^{-14}$	$2.02 \cdot 10^{-14}$
3	$1.80 \cdot 10^{-14}$	$1.94 \cdot 10^{-14}$	$1.90 \cdot 10^{-14}$
4	$1.79 \cdot 10^{-14}$	$1.86 \cdot 10^{-14}$	$1.94 \cdot 10^{-14}$
5	$1.80 \cdot 10^{-14}$	$1.86 \cdot 10^{-14}$	$1.86 \cdot 10^{-14}$

value [22] of  $2.06 \cdot 10^{-11} \text{ cm}^3 \text{ molecule}^{-1} \text{ s}^{-1}$  shows a satisfying agreement between calculations and the experiment.

### 3.2. Reactions of Chlorine Atoms with Hydrogen Molecules



This reaction is endothermic with a barrier energy of 0.172 eV at  $J = 0$ . The calculated probabilities and reaction cross-sections for this reaction at several  $v$  and  $J$  values are shown in Table 3. The calculated reaction rate constants are shown in Table 4. Variations

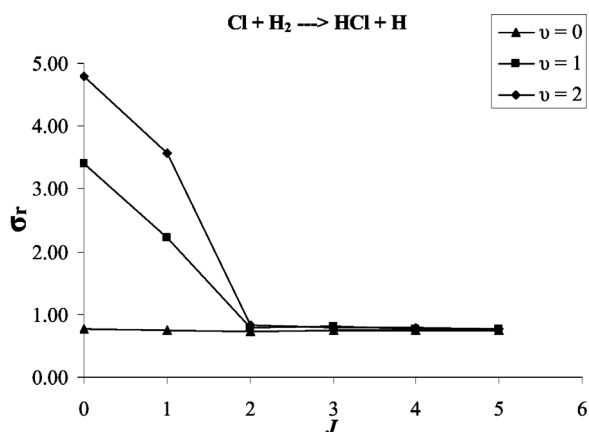


Fig. 2. Variation of the reaction cross-section  $\sigma_r$  for the reaction  $\text{Cl} + \text{H}_2 \rightarrow \text{HCl} + \text{H}$  with both  $v$  and  $J$  values.

of the reaction cross-section with both  $v$  and  $J$  values are shown in Figure 2. The same behaviour is observed regarding the variation of the reaction cross-section with the initial vibrational quantum number of the  $\text{H}_2$  molecule; the reaction rate increases as the vibrational state of molecule increases. The effect of  $J$ , for  $v = 0$ , is the same as before, i. e. minor contribution of  $J$  values on the rates is observed. However, as shown in Fig. 2, the rates drop sharply with the first few  $J$  values for  $v = 1, 2$ . For a small molecule like  $\text{H}_2$ , higher rotational velocity at higher vibrational velocity lowers the collision probability, and hence the reaction rate. This reaction between a Cl atom and a  $\text{H}_2$  molecule had been studied theoretically by other investigators [23, 24]. Comparing their rate constants with ours, reported earlier [1], shows good agreement over a wide temperature range (200 K – 1000 K).

### 3.3. Reactions of Chlorine Atoms with HD Molecules



The reaction of Cl with HD is an endothermic process. It has a barrier energy that has to be considered in the calculations of the rate constant [equation (7)]. The barrier energy reported in the literature varies with the rotational quantum number for the molecule. The calculated probabilities at various  $v$  and  $J$  values are shown in Table 5 and the corresponding reaction rate constants are shown in Table 6. Variations of the reaction cross-section and rate constant with both  $v$  and  $J$  values are shown in Figs. 3 and 4, respectively. The same trend is observed here. The reaction cross-

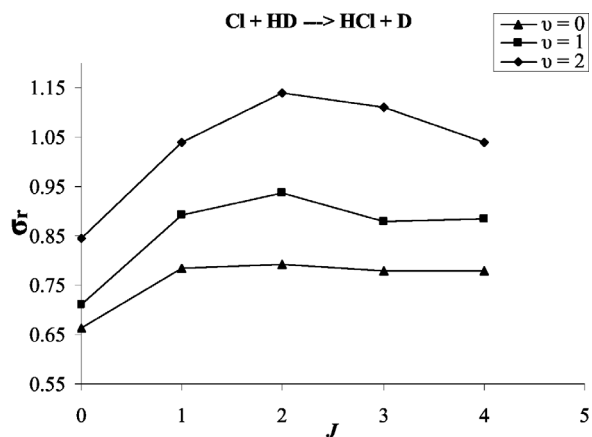


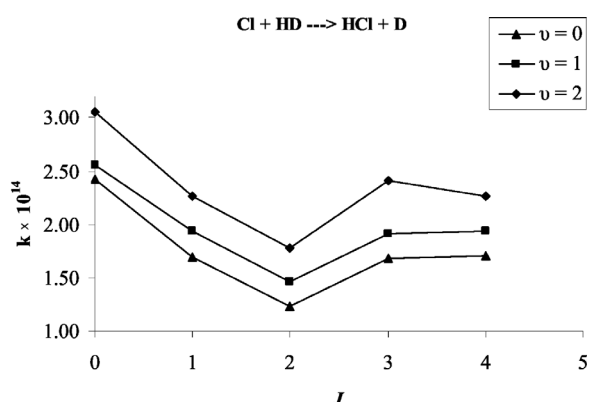
Fig. 3. Variation of the reaction cross-section  $\sigma_r$  for the reaction  $\text{Cl} + \text{HD} \rightarrow \text{HCl} + \text{D}$  with both  $v$  and  $J$  values.

Table 5. Calculated probabilities  $[P(T)]$  and reaction cross-sections ( $\sigma_r$ ), in  $\text{\AA}^2$ , for the reaction  $\text{Cl} + \text{HD} \rightarrow \text{HCl} + \text{D}$  at various  $\nu$  and  $J$  values.

$J$	$\nu = 0$		$\nu = 1$		$\nu = 2$	
	$P(T)$	$\sigma_r$	$P(T)$	$\sigma_r$	$P(T)$	$\sigma_r$
0	0.0704	0.663	0.0754	0.710	0.0898	0.845
1	0.0833	0.784	0.0946	0.891	0.110	1.04
2	0.0841	0.792	0.0994	0.936	0.121	1.14
3	0.0826	0.778	0.0932	0.878	0.117	1.11
4	0.0827	0.779	0.0940	0.885	0.110	1.04

Table 6. Calculated reaction rate constants  $[k(T)]$  for the reaction  $\text{Cl} + \text{HD} \rightarrow \text{HCl} + \text{D}$  at various  $\nu$  and  $J$  values.

$J$	$k(T)$ [ $\text{cm}^3 \text{ molecule}^{-1} \text{ s}^{-1}$ ]		
	$\nu = 0$	$\nu = 1$	$\nu = 2$
0	$2.42 \cdot 10^{-14}$	$2.56 \cdot 10^{-14}$	$3.05 \cdot 10^{-14}$
1	$1.69 \cdot 10^{-14}$	$1.94 \cdot 10^{-14}$	$2.26 \cdot 10^{-14}$
2	$1.23 \cdot 10^{-14}$	$1.46 \cdot 10^{-14}$	$1.78 \cdot 10^{-14}$
3	$1.68 \cdot 10^{-14}$	$1.91 \cdot 10^{-14}$	$2.41 \cdot 10^{-14}$
4	$1.71 \cdot 10^{-14}$	$1.93 \cdot 10^{-14}$	$2.27 \cdot 10^{-14}$

Fig. 4. Variation of the reaction rate constant  $k$  for the reaction  $\text{Cl} + \text{HD} \rightarrow \text{HCl} + \text{D}$  with both  $\nu$  and  $J$  values.

sections and rate constants increase with the vibrational quantum number  $\nu$ . However, within the same  $\nu$ , the reaction probability increases with  $J$  to reach a maximum at  $J = 2$ ; then it drops or levels out. Regarding the rate constant, it is higher for lower  $J$  values, and it reaches a minimum at  $J = 2$ . Then, it starts to rise and levels out at higher  $J$  values. This variation of the rate constant is due to a variation of the barrier energy with  $J$  values. The values of the barrier energy  $E_0$  at  $J = 0, 2, 4$  are equal to 0.156, 0.178, and 0.169 eV, respectively.

#### B) $\text{Cl} + \text{HD} \rightarrow \text{DCI} + \text{H}$

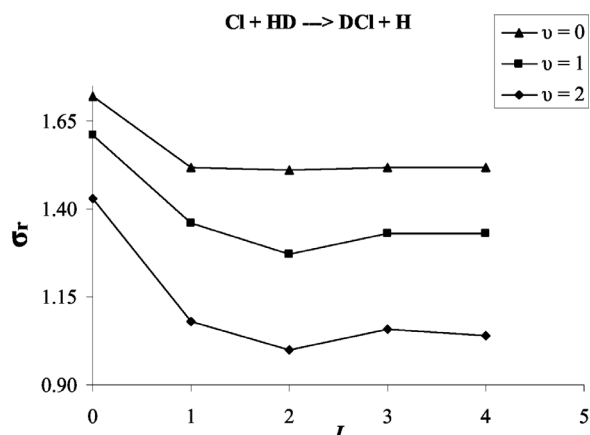
This reaction is like the previous one an endothermic process. The barrier energy increases with the rotational quantum number of the molecule. The values re-

Table 7. Calculated probabilities  $[P(T)]$  and reaction cross-sections ( $\sigma_r$ ), in  $\text{\AA}^2$ , for the reaction  $\text{Cl} + \text{HD} \rightarrow \text{DCI} + \text{H}$  at various  $\nu$  and  $J$  values.

$J$	$\nu = 0$		$\nu = 1$		$\nu = 2$	
	$P(T)$	$\sigma_r$	$P(T)$	$\sigma_r$	$P(T)$	$\sigma_r$
0	0.182	1.72	0.171	1.61	0.152	1.43
1	0.162	1.52	0.144	1.36	0.115	1.08
2	0.161	1.51	0.135	1.27	0.107	1.00
3	0.161	1.52	0.141	1.33	0.112	1.06
4	0.162	1.52	0.141	1.33	0.110	1.04

Table 8. Calculated reaction rate constants  $[k(T)]$  for the reaction  $\text{Cl} + \text{HD} \rightarrow \text{DCI} + \text{H}$  at various  $\nu$  and  $J$  values.

$J$	$k(T)$ [ $\text{cm}^3 \text{ molecule}^{-1} \text{ s}^{-1}$ ]		
	$\nu = 0$	$\nu = 1$	$\nu = 2$
0	$7.82 \cdot 10^{-15}$	$7.34 \cdot 10^{-15}$	$6.53 \cdot 10^{-15}$
1	$4.69 \cdot 10^{-15}$	$4.21 \cdot 10^{-15}$	$3.35 \cdot 10^{-15}$
2	$4.37 \cdot 10^{-15}$	$3.70 \cdot 10^{-15}$	$2.92 \cdot 10^{-15}$
3	$1.36 \cdot 10^{-15}$	$1.20 \cdot 10^{-15}$	$9.53 \cdot 10^{-16}$
4	$8.18 \cdot 10^{-16}$	$7.22 \cdot 10^{-16}$	$5.64 \cdot 10^{-16}$

Fig. 5. Variation of the reaction cross-section  $\sigma_r$  for the reaction  $\text{Cl} + \text{HD} \rightarrow \text{DCI} + \text{H}$  with both  $\nu$  and  $J$  values.

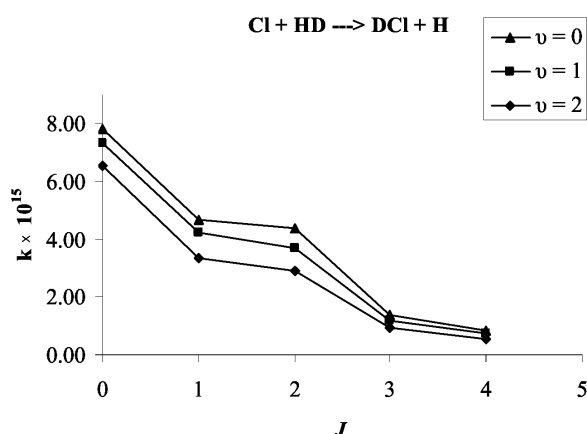
ported in the literature for its barrier energy  $E_0$  at  $J = 0, 2, 4$  are: 0.210, 0.221, and 0.265 eV, respectively. The calculated probabilities at various  $\nu$  and  $J$  values are shown in Table 7 and the corresponding reaction rate constants are shown in Table 8. Variations of the reaction cross-section and rate constant with both  $\nu$  and  $J$  values are shown in Figs. 5 and 6, respectively. For this reaction, the probabilities and reaction cross-sections are generally higher than those for the competing reaction  $\text{Cl} + \text{HD} \rightarrow \text{HCl} + \text{D}$  (cf. A). However, the rate constants are an order of magnitude smaller than those for the competing reaction. This is due to higher barrier energies for the formation of DCI compared to the formation of HCl. The variation of the reaction cross-section and rate constant with both  $\nu$  and  $J$  values

Table 9. Calculated rate constants [ $k(T)$ ] for the reaction  $\text{Cl} + \text{HD} \rightarrow \text{HCl} + \text{D}$  at different temperatures for various rotational quantum numbers ( $J$ ) in  $\text{cm}^3 \text{molecules}^{-1} \text{s}^{-1}$ .

T/K	$J=0$ $E_0 = 0.156 \text{ eV}$ $k(T)$		$J=1$ $E_0 = 0.169 \text{ eV}$ $k(T)$		$J=2$ $E_0 = 0.178 \text{ eV}$ $k(T)$		$J=3$ $E_0 = 0.169 \text{ eV}$ $k(T)$		$J=4$ $E_0 = 0.169 \text{ eV}$ $k(T)$	
	This work	[3]	This work	[3]	This work	[3]	This work	[3]	This work	[3]
	250	$6.61 \cdot 10^{-15}$	$5.73 \cdot 10^{-15}$	$4.46 \cdot 10^{-15}$	$3.06 \cdot 10^{-15}$	$2.92 \cdot 10^{-15}$	$1.50 \cdot 10^{-15}$	$4.19 \cdot 10^{-15}$	$2.03 \cdot 10^{-15}$	$4.40 \cdot 10^{-15}$
300	$2.42 \cdot 10^{-14}$	$2.23 \cdot 10^{-14}$	$1.69 \cdot 10^{-14}$	$1.34 \cdot 10^{-14}$	$1.23 \cdot 10^{-14}$	$0.722 \cdot 10^{-14}$	$1.68 \cdot 10^{-14}$	$0.842 \cdot 10^{-14}$	$1.71 \cdot 10^{-14}$	$1.15 \cdot 10^{-14}$
400	$1.24 \cdot 10^{-13}$	$1.29 \cdot 10^{-13}$	$9.39 \cdot 10^{-14}$	$8.72 \cdot 10^{-14}$	$7.36 \cdot 10^{-14}$	$5.51 \cdot 10^{-14}$	$9.46 \cdot 10^{-14}$	$6.13 \cdot 10^{-14}$	$9.53 \cdot 10^{-14}$	$7.59 \cdot 10^{-14}$
500	$3.46 \cdot 10^{-13}$	$3.87 \cdot 10^{-13}$	$2.76 \cdot 10^{-13}$	$2.72 \cdot 10^{-13}$	$2.26 \cdot 10^{-13}$	$1.98 \cdot 10^{-13}$	$2.73 \cdot 10^{-13}$	$2.01 \cdot 10^{-13}$	$2.77 \cdot 10^{-13}$	$2.47 \cdot 10^{-13}$

Table 10. Calculated rate constants [ $k(T)$ ] for the reaction  $\text{Cl} + \text{HD} \rightarrow \text{DCl} + \text{H}$  at different temperatures for various rotational quantum numbers ( $J$ ) in  $\text{cm}^3 \text{molecules}^{-1} \text{s}^{-1}$ .

T/K	$J=0$ $E_0 = 0.210 \text{ eV}$ $k(T)$		$J=1$ $E_0 = 0.220 \text{ eV}$ $k(T)$		$J=2$ $E_0 = 0.221 \text{ eV}$ $k(T)$		$J=3$ $E_0 = 0.252 \text{ eV}$ $k(T)$		$J=4$ $E_0 = 0.265 \text{ eV}$ $k(T)$	
	This work	[3]	This work	[3]	This work	[3]	This work	[3]	This work	[3]
	250	$1.48 \cdot 10^{-15}$	$1.76 \cdot 10^{-15}$	$0.815 \cdot 10^{-15}$	$1.25 \cdot 10^{-15}$	$7.57 \cdot 10^{-16}$	$4.17 \cdot 10^{-16}$	$1.86 \cdot 10^{-16}$	$0.717 \cdot 10^{-16}$	$1.00 \cdot 10^{-16}$
300	$7.82 \cdot 10^{-15}$	$8.95 \cdot 10^{-15}$	$4.69 \cdot 10^{-15}$	$6.54 \cdot 10^{-15}$	$4.37 \cdot 10^{-15}$	$2.64 \cdot 10^{-15}$	$1.36 \cdot 10^{-15}$	$0.756 \cdot 10^{-15}$	$8.18 \cdot 10^{-16}$	$3.02 \cdot 10^{-16}$
400	$6.62 \cdot 10^{-14}$	$7.27 \cdot 10^{-14}$	$4.24 \cdot 10^{-14}$	$6.19 \cdot 10^{-14}$	$4.04 \cdot 10^{-14}$	$3.22 \cdot 10^{-14}$	$1.69 \cdot 10^{-14}$	$1.14 \cdot 10^{-14}$	$1.15 \cdot 10^{-14}$	$0.603 \cdot 10^{-14}$
500	$2.22 \cdot 10^{-13}$	$2.67 \cdot 10^{-13}$	$1.63 \cdot 10^{-13}$	$2.39 \cdot 10^{-13}$	$1.54 \cdot 10^{-13}$	$1.44 \cdot 10^{-13}$	$7.72 \cdot 10^{-14}$	$6.61 \cdot 10^{-14}$	$5.58 \cdot 10^{-14}$	$3.94 \cdot 10^{-14}$

Fig. 6. Variation of the reaction rate constant  $k$  for the reaction  $\text{Cl} + \text{HD} \rightarrow \text{DCl} + \text{H}$  with both  $v$  and  $J$  values.

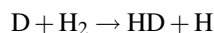
has a totally different trend compared with what is observed for all of the above reactions. The reaction probability, cross-section and rate constant decrease as the molecule goes to higher vibrational levels. Also, within the same vibrational level, they decrease as  $J$  increases. This trend is due to the possibility of the occurrence of the competing reaction (cf. A). Higher vibrational and rotational excitations favour the formation of the competing HCl molecule at the expense of DCl formation.

One more thing can be said about these two reactions; due to the higher endothermicity of the DCl formation, its rate constant varies significantly with both  $v$  and  $J$ , compared with minor changes during HCl

formation. A comparison can also be made with results obtained for the reaction  $\text{Cl} + \text{H}_2 \rightarrow \text{HCl} + \text{H}$  discussed before. The spectroscopic constants and Morse potentials for this reaction predict intermediate values for its reaction rate constant (Table 4) compared with the rates for the reactions  $\text{Cl} + \text{HD} \rightarrow \text{HCl} + \text{D}$  and  $\text{Cl} + \text{HD} \rightarrow \text{DCl} + \text{H}$  (Tables 6 and 8).

The above two reactions ( $\text{Cl} + \text{HD} \rightarrow \text{HCl} + \text{D}$  and  $\text{Cl} + \text{HD} \rightarrow \text{DCl} + \text{H}$ ) had been studied in detail by Persky [3] using different calculation methods. The rate constant was calculated at different temperatures for various  $J$  values. For comparison purposes, we performed our calculations for the rate constants to the same conditions as Persky. The results are shown in Tables 9 and 10. The agreement between our rate constants and Persky's one is obvious. Plots of the variation of the rate constant with  $J$  at various temperatures are shown in Figs. 7a and 7b for the HCl production and in Figs. 8a and 8b for the DCl production. The same trend for the variation of the rate constant with  $J$  is observed for both works indicating the reliability of our calculation method.

### 3.4. Reactions of Deuterium Atoms with Hydrogen Molecules



The calculated probabilities and reaction cross-sections for this reaction at several  $v$  and  $J$  values are

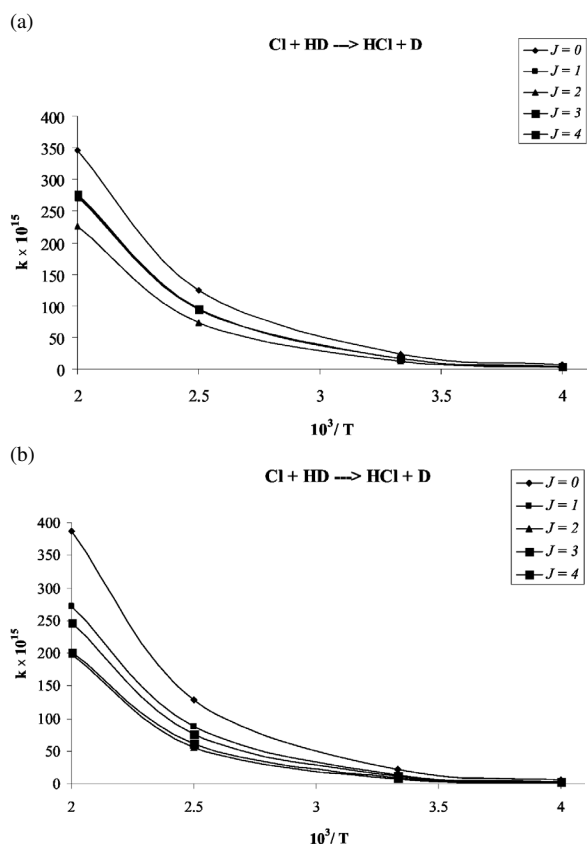


Fig. 7. Variation of the reaction rate constant  $k$  for the reaction  $\text{Cl} + \text{HD} \rightarrow \text{HCl} + \text{D}$  with  $J$  values at various temperatures. (a) Results obtained in the present work. (b) Results obtained by other investigators [3].

shown in Table 11. The calculated reaction rate constants are shown in Table 12. Variations of the reaction cross-section with both  $v$  and  $J$  values are plotted in Fig. 9, which shows that, in general, the reaction cross-section increases with both vibrational and rotational quantum numbers of the  $\text{H}_2$  molecule. As the molecule gets more vibrational and rotational excitation, its bond weakens and hence, it becomes more likely to react. This leads to a higher reaction cross-section.

Comparing the rates of this reaction with those for the reaction  $\text{Cl} + \text{H}_2 \rightarrow \text{HCl} + \text{H}$  shows higher reaction probabilities and cross-sections for the latter reaction due to a deeper potential well for the  $\text{HCl}$  formation compared to  $\text{DH}$  formation. However, the rate constants for that reaction are about three orders of magnitude smaller than those for the reaction  $\text{D} + \text{H}_2 \rightarrow \text{HD} + \text{H}$ . This is due to the endothermicity of the  $\text{HCl}$  formation.

Table 11. Calculated probabilities  $[P(T)]$  and reaction cross-sections ( $\sigma_r$ ), in  $\text{\AA}^2$ , for the reaction  $\text{D} + \text{H}_2 \rightarrow \text{HD} + \text{H}$  at various  $v$  and  $J$  values.

$J$	$v = 0$		$v = 1$		$v = 2$	
	$P(T)$	$\sigma_r$	$P(T)$	$\sigma_r$	$P(T)$	$\sigma_r$
0	0.0342	0.133	0.0354	0.137	0.0408	0.159
1	0.0329	0.128	0.0351	0.136	0.0391	0.152
2	0.0337	0.131	0.0340	0.132	0.0383	0.149
3	0.0361	0.140	0.0379	0.147	0.0401	0.156
4	0.0365	0.142	0.0374	0.145	0.0406	0.158
5	0.0371	0.144	0.0375	0.146	0.0412	0.160
6	0.0370	0.144	0.0381	0.148	0.0417	0.162
7	0.0375	0.146	0.0395	0.154	0.0426	0.166
8	0.0385	0.150	0.0398	0.155	0.0424	0.165
9	0.0396	0.154	0.0386	0.150	0.0437	0.170
10	0.0402	0.156	0.0405	0.157	0.0448	0.174
11	0.0400	0.155	0.0432	0.168	0.0439	0.171
12	0.0405	0.157	0.0449	0.174	0.0477	0.186

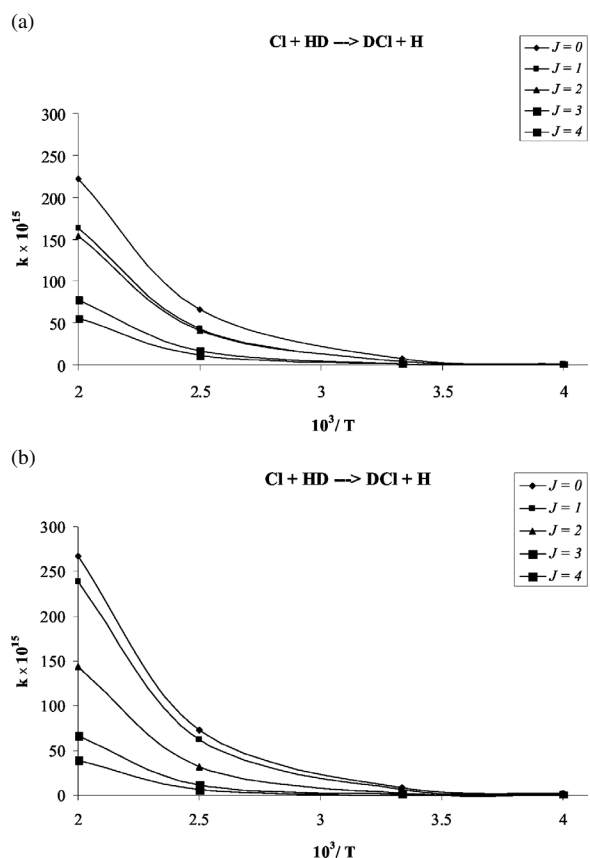


Fig. 8. Variation of the reaction rate constant  $k$  for the reaction  $\text{Cl} + \text{HD} \rightarrow \text{DCl} + \text{H}$  with  $J$  values at various temperatures. (a) Results obtained in the present work. (b) Results obtained by other investigators [3].

Effects of translational, rotational, and vibrational energies on the dynamics of this exchange reaction had

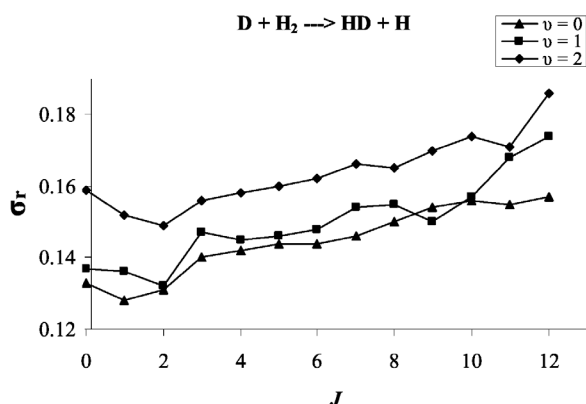


Fig. 9. Variation of the reaction cross-section  $\sigma_r$  for the reaction  $D + H_2 \rightarrow HD + H$  with both  $\nu$  and  $J$  values.

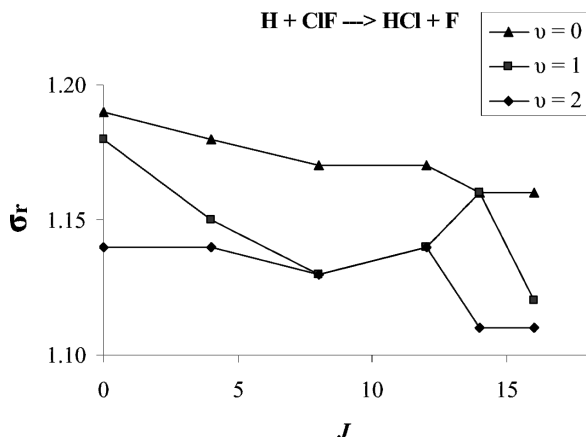


Fig. 10. Variation of the reaction cross-section  $\sigma_r$  for the reaction  $H + ClF \rightarrow HCl + F$  with both  $\nu$  and  $J$  values.

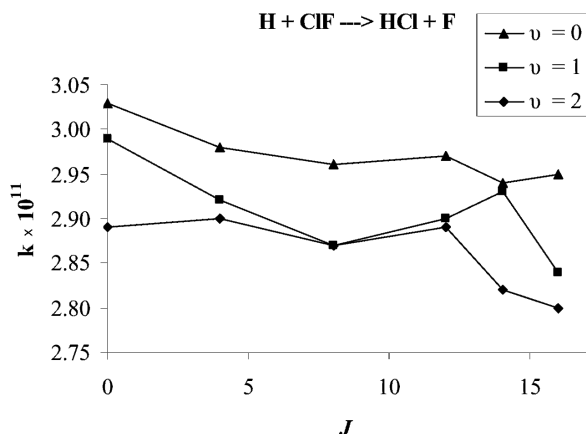


Fig. 11. Variation of the reaction rate constant  $k$  for the reaction  $H + ClF \rightarrow HCl + F$  with both  $\nu$  and  $J$  values.

been extensively studied by Aoiz et al. [9] using QCT calculations. They used a LSTH potential energy sur-

Table 12. Calculated reaction rate constants  $[k(T)]$  for the reaction  $D + H_2 \rightarrow HD + H$  at various  $\nu$  and  $J$  values.

$J$	$k(T)$ [ $\text{cm}^3 \text{ molecule}^{-1} \text{ s}^{-1}$ ]		
	$\nu = 0$	$\nu = 1$	$\nu = 2$
0	$1.00 \cdot 10^{-11}$	$1.04 \cdot 10^{-11}$	$1.20 \cdot 10^{-11}$
1	$9.65 \cdot 10^{-12}$	$1.03 \cdot 10^{-11}$	$1.15 \cdot 10^{-11}$
2	$9.91 \cdot 10^{-12}$	$9.98 \cdot 10^{-12}$	$1.13 \cdot 10^{-11}$
3	$1.06 \cdot 10^{-11}$	$1.11 \cdot 10^{-11}$	$1.18 \cdot 10^{-11}$
4	$1.07 \cdot 10^{-11}$	$1.10 \cdot 10^{-11}$	$1.19 \cdot 10^{-11}$
5	$1.09 \cdot 10^{-11}$	$1.10 \cdot 10^{-11}$	$1.21 \cdot 10^{-11}$
6	$1.09 \cdot 10^{-11}$	$1.12 \cdot 10^{-11}$	$1.22 \cdot 10^{-11}$
7	$1.10 \cdot 10^{-11}$	$1.16 \cdot 10^{-11}$	$1.25 \cdot 10^{-11}$
8	$1.13 \cdot 10^{-11}$	$1.17 \cdot 10^{-11}$	$1.25 \cdot 10^{-11}$
9	$1.16 \cdot 10^{-11}$	$1.13 \cdot 10^{-11}$	$1.28 \cdot 10^{-11}$
10	$1.18 \cdot 10^{-11}$	$1.19 \cdot 10^{-11}$	$1.32 \cdot 10^{-11}$
11	$1.17 \cdot 10^{-11}$	$1.27 \cdot 10^{-11}$	$1.29 \cdot 10^{-11}$
12	$1.19 \cdot 10^{-11}$	$1.32 \cdot 10^{-11}$	$1.40 \cdot 10^{-11}$

Table 13. Calculated probabilities  $[P(T)]$  and reaction cross-sections ( $\sigma_r$ ), in  $\text{\AA}^2$ , for the reaction  $H + ClF \rightarrow HCl + F$  at various  $\nu$  and  $J$  values.

$J$	$\nu = 0$		$\nu = 1$		$\nu = 2$	
	$P(T)$	$\sigma_r$	$P(T)$	$\sigma_r$	$P(T)$	$\sigma_r$
0	0.0953	1.19	0.0942	1.18	0.0911	1.14
4	0.0937	1.18	0.0920	1.15	0.0912	1.14
8	0.0932	1.17	0.0902	1.13	0.0902	1.13
12	0.0934	1.17	0.0912	1.14	0.0910	1.14
14	0.0926	1.16	0.0921	1.16	0.0887	1.11
16	0.0927	1.16	0.0894	1.12	0.0882	1.11

face to study the combined effects of translation, rotation, and vibration on the reactivity. Their findings showed that the total reaction cross-section increases as the rotational and vibrational energy of the molecule ( $H_2$ ) increases. This is in accord with our findings in the present work.

### 3.5. Reactions of Hydrogen Atoms with ClF Molecules

#### A) $H + ClF \rightarrow HCl + F$

The calculated probabilities and reaction cross-sections for this reaction at several  $\nu$  and  $J$  values are shown in Table 13. The calculated reaction rate constants are shown in Table 14. Variations of the reaction cross-section and rate constant with both  $\nu$  and  $J$  values are shown in Figs. 10 and 11, respectively.

#### B) $H + ClF \rightarrow HF + Cl$

The calculated probabilities and reaction cross-sections for this reaction at several  $\nu$  and  $J$  values are shown in Table 15. The calculated rate constants are

Table 14. Calculated reaction rate constants  $[k(T)]$  for the reaction  $\text{H} + \text{ClF} \rightarrow \text{HCl} + \text{F}$  at various  $\nu$  and  $J$  values.

$J$	$k(T)$ [ $\text{cm}^3 \text{ molecule}^{-1} \text{ s}^{-1}$ ]		
	$\nu = 0$	$\nu = 1$	$\nu = 2$
0	$3.03 \cdot 10^{-11}$	$2.99 \cdot 10^{-11}$	$2.89 \cdot 10^{-11}$
4	$2.98 \cdot 10^{-11}$	$2.92 \cdot 10^{-11}$	$2.90 \cdot 10^{-11}$
8	$2.96 \cdot 10^{-11}$	$2.87 \cdot 10^{-11}$	$2.87 \cdot 10^{-11}$
12	$2.97 \cdot 10^{-11}$	$2.90 \cdot 10^{-11}$	$2.89 \cdot 10^{-11}$
14	$2.94 \cdot 10^{-11}$	$2.93 \cdot 10^{-11}$	$2.82 \cdot 10^{-11}$
16	$2.95 \cdot 10^{-11}$	$2.84 \cdot 10^{-11}$	$2.80 \cdot 10^{-11}$

Table 15. Calculated probabilities  $[P(T)]$  and reaction cross-sections ( $\sigma_r$ ), in  $\text{\AA}^2$ , for the reaction  $\text{H} + \text{ClF} \rightarrow \text{HF} + \text{Cl}$  at various  $\nu$  and  $J$  values.

$J$	$\nu = 0$		$\nu = 1$		$\nu = 2$	
	$P(T)$	$\sigma_r$	$P(T)$	$\sigma_r$	$P(T)$	$\sigma_r$
0	0.0361	0.452	0.0362	0.454	0.0344	0.431
4	0.0366	0.459	0.0368	0.462	0.0348	0.436
8	0.0361	0.452	0.0347	0.435	0.0344	0.431
12	0.0334	0.419	0.0335	0.421	0.0332	0.417
14	0.0343	0.431	0.0320	0.401	0.0341	0.428
16	0.0323	0.406	0.0303	0.380	0.0338	0.424

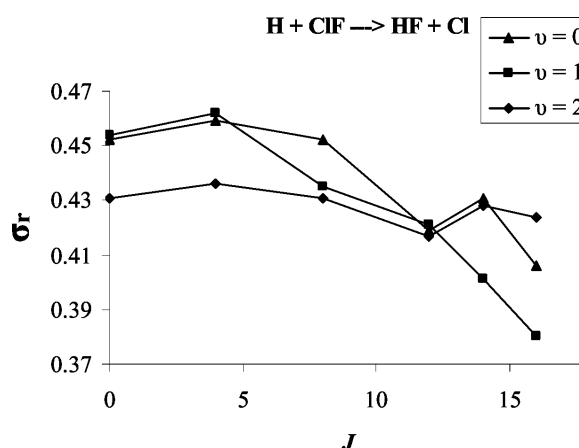
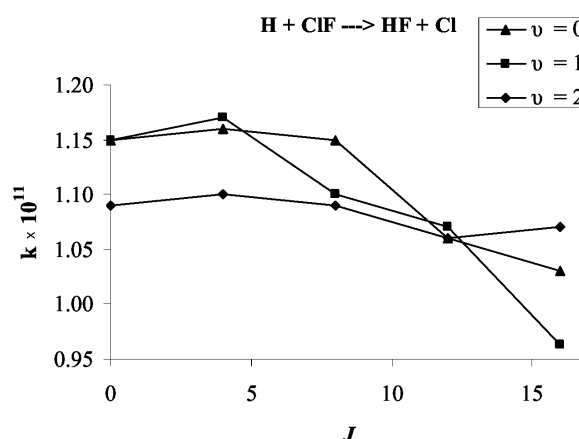
Table 16. Calculated reaction rate constants  $[k(T)]$  for the reaction  $\text{H} + \text{ClF} \rightarrow \text{HF} + \text{Cl}$  at various  $\nu$  and  $J$  values.

$J$	$k(T)$ [ $\text{cm}^3 \text{ molecule}^{-1} \text{ s}^{-1}$ ]		
	$\nu = 0$	$\nu = 1$	$\nu = 2$
0	$1.15 \cdot 10^{-11}$	$1.15 \cdot 10^{-11}$	$1.09 \cdot 10^{-11}$
4	$1.16 \cdot 10^{-11}$	$1.17 \cdot 10^{-11}$	$1.10 \cdot 10^{-11}$
8	$1.15 \cdot 10^{-11}$	$1.10 \cdot 10^{-11}$	$1.09 \cdot 10^{-11}$
12	$1.06 \cdot 10^{-11}$	$1.07 \cdot 10^{-11}$	$1.06 \cdot 10^{-11}$
14	$1.09 \cdot 10^{-11}$	$1.02 \cdot 10^{-11}$	$1.08 \cdot 10^{-11}$
16	$1.03 \cdot 10^{-11}$	$9.63 \cdot 10^{-12}$	$1.07 \cdot 10^{-11}$

shown in Table 16. Variations of the reaction cross-section with both  $\nu$  and  $J$  values are shown in Figs. 12 and 13, respectively.

### C) $\text{H} + \text{ClF} \rightarrow \text{HCl} + \text{F}$ vs. $\text{H} + \text{ClF} \rightarrow \text{HF} + \text{Cl}$

The two competing reactions have the same colliding particles, but form different products: HCl and HF molecules. Therefore, it makes sense to compare the probabilities of formation of the two molecules (HCl vs. HF). The calculations for the formation of the two molecules were performed under the same initial conditions and showed that the variation of the reaction probability, cross-section and rate constant, for both reactions, with both  $\nu$  and  $J$  values are minor. However, at a given  $\nu$  and  $J$  value, the probability of HCl formation is almost *three* times higher than the corresponding value for HF formation. This is due to the difference in the potential of the HCl and HF molecules. Looking at (3), with  $D_{\text{HCl}}$  is generally smaller than  $D_{\text{HF}}$ , it gives a poten-

Fig. 12. Variation of the reaction cross-section  $\sigma_r$  for the reaction  $\text{H} + \text{ClF} \rightarrow \text{HF} + \text{Cl}$  with both  $\nu$  and  $J$  values.Fig. 13. Variation of the reaction rate constant  $k$  for the reaction  $\text{H} + \text{ClF} \rightarrow \text{HF} + \text{Cl}$  with both  $\nu$  and  $J$  values.

tial value for  $V_{\text{HCl}}$  which is higher than that for  $V_{\text{HF}}$  at any distance throughout the trajectory. This means a stronger attraction, and hence a favourable formation of HCl molecules over HF molecules. This is in agreement with the experimental result. At  $\nu = 0$  and  $J = J_{\text{max}}$ , the experimental [25] ratio of the rate constants for the formation of HCl vs. HF is the same as the calculated ratio. Also, the same agreement is observed in the experimental findings reported by Tamagake and Setser [26]. From the relative infrared emission intensities of HCl and HF produced by the  $\text{H} + \text{ClF}$  reaction, they found a macroscopic branching ratio of 5.20 favouring the HCl channel. Comparing our calculated rate constant with other calculated values [1, 27] shows a reasonable agreement.

Table 17. Calculated probabilities [ $P(T)$ ] and reaction cross-sections ( $\sigma_r$ ), in  $\text{\AA}^2$ , for the reaction  $\text{H} + \text{HCl} \rightarrow \text{H}_2 + \text{Cl}$  at various  $v$  and  $J$  values.

$J$	$v=0$		$v=1$		$v=2$	
	$P(T)$	$\sigma_r$	$P(T)$	$\sigma_r$	$P(T)$	$\sigma_r$
0	0.00283	0.0240	0.00358	0.0304	0.00568	0.0483
1	0.00327	0.0278	0.00328	0.0279	0.00549	0.0467
2	0.00272	0.0231	0.00434	0.0369	0.00545	0.0463
3	0.00245	0.0208	0.00348	0.0296	0.00457	0.0388
4	0.00328	0.0278	0.00348	0.0296	0.00528	0.0449

Table 18. Calculated reaction rate constants [ $k(T)$ ] for the reaction  $\text{H} + \text{HCl} \rightarrow \text{H}_2 + \text{Cl}$  at various  $v$  and  $J$  values.

$J$	$k(T)$ [ $\text{cm}^3 \text{ molecule}^{-1} \text{ s}^{-1}$ ]		
	$v=0$	$v=1$	$v=2$
0	$6.11 \cdot 10^{-13}$	$7.74 \cdot 10^{-13}$	$1.23 \cdot 10^{-12}$
1	$7.08 \cdot 10^{-13}$	$7.09 \cdot 10^{-13}$	$1.19 \cdot 10^{-12}$
2	$5.88 \cdot 10^{-13}$	$9.38 \cdot 10^{-13}$	$1.18 \cdot 10^{-12}$
3	$5.29 \cdot 10^{-13}$	$7.52 \cdot 10^{-13}$	$9.88 \cdot 10^{-13}$
4	$7.09 \cdot 10^{-13}$	$7.53 \cdot 10^{-13}$	$1.14 \cdot 10^{-12}$

Table 19. Calculated probabilities [ $P(T)$ ] and reaction cross-sections ( $\sigma_r$ ), in  $\text{\AA}^2$ , for the reaction  $\text{H} + \text{HCl} \rightarrow \text{HCl} + \text{H}$  at various  $v$  and  $J$  values.

$J$	$v=0$		$v=1$		$v=2$	
	$P(T)$	$\sigma_r$	$P(T)$	$\sigma_r$	$P(T)$	$\sigma_r$
0	0.0316	0.269	0.0339	0.288	0.0357	0.303
1	0.0327	0.278	0.0346	0.294	0.0350	0.297
2	0.0324	0.275	0.0344	0.292	0.0355	0.302
3	0.0312	0.265	0.0348	0.296	0.0359	0.305
4	0.0319	0.271	0.0350	0.297	0.0345	0.293

### 3.6. Reactions of Hydrogen Atoms with HCl Molecules

#### A) $\text{H} + \text{HCl} \rightarrow \text{H}_2 + \text{Cl}$

The calculated probabilities and reaction cross-sections for this reaction at several  $v$  and  $J$  values are shown in Table 17. The calculated reaction rate constants are shown in Table 18. Variations of the reaction cross-section and rate constant with both  $v$  and  $J$  values are shown in Figs. 14 and 15, respectively.

#### B) $\text{H} + \text{HCl} \rightarrow \text{HCl} + \text{H}$

Even though there is no weight change in this process, however, it involves breakage of the H-Cl bond and an exchange of H atoms occurs. The calculated probabilities and reaction cross-sections for this reaction at several  $v$  and  $J$  values are shown in Table 19. The calculated reaction rate constants are shown in Table 20. Variations of the reaction cross-section with both  $v$  and  $J$  values are shown in Figs. 16 and 17, respectively.

Table 20. Calculated reaction rate constants [ $k(T)$ ] for the reaction  $\text{H} + \text{HCl} \rightarrow \text{HCl} + \text{H}$  at various  $v$  and  $J$  values.

$J$	$k(T)$ [ $\text{cm}^3 \text{ molecule}^{-1} \text{ s}^{-1}$ ]		
	$v=0$	$v=1$	$v=2$
0	$6.84 \cdot 10^{-12}$	$7.32 \cdot 10^{-12}$	$7.71 \cdot 10^{-12}$
1	$7.07 \cdot 10^{-12}$	$7.49 \cdot 10^{-12}$	$7.56 \cdot 10^{-12}$
2	$7.00 \cdot 10^{-12}$	$7.44 \cdot 10^{-12}$	$7.68 \cdot 10^{-12}$
3	$6.74 \cdot 10^{-12}$	$7.52 \cdot 10^{-12}$	$7.77 \cdot 10^{-12}$
4	$6.90 \cdot 10^{-12}$	$7.56 \cdot 10^{-12}$	$7.46 \cdot 10^{-12}$

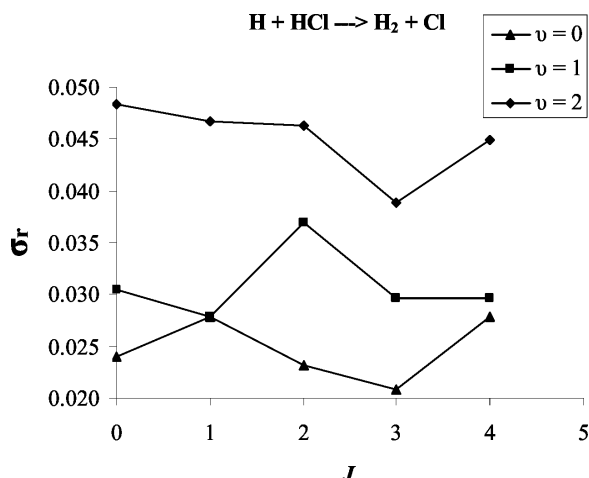


Fig. 14. Variation of the reaction cross-section  $\sigma_r$  for the reaction  $\text{H} + \text{HCl} \rightarrow \text{H}_2 + \text{Cl}$  with both  $v$  and  $J$  values.

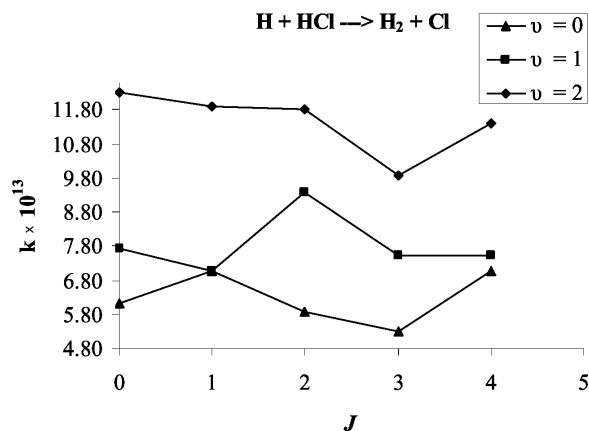


Fig. 15. Variation of the reaction rate constant  $k$  for the reaction  $\text{H} + \text{HCl} \rightarrow \text{H}_2 + \text{Cl}$  with both  $v$  and  $J$  values.

#### C) $\text{H} + \text{HCl} \rightarrow \text{H}_2 + \text{Cl}$ vs. $\text{H} + \text{HCl} \rightarrow \text{HCl} + \text{H}$

For both processes, the reaction cross-section increases with  $v$  but varies slightly with  $J$  values. However, the reaction probabilities, cross-sections and rate constants for the first process are an order of magnitude smaller than that for the second. The two competing reactions are in favour of the “formation” of HCl

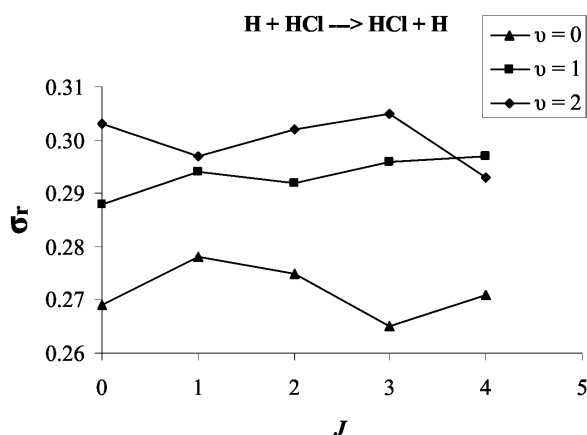


Fig. 16. Variation of the reaction cross-section  $\sigma_r$  for the reaction  $\text{H} + \text{HCl} \rightarrow \text{HCl} + \text{H}$  with both  $\nu$  and  $J$  values.

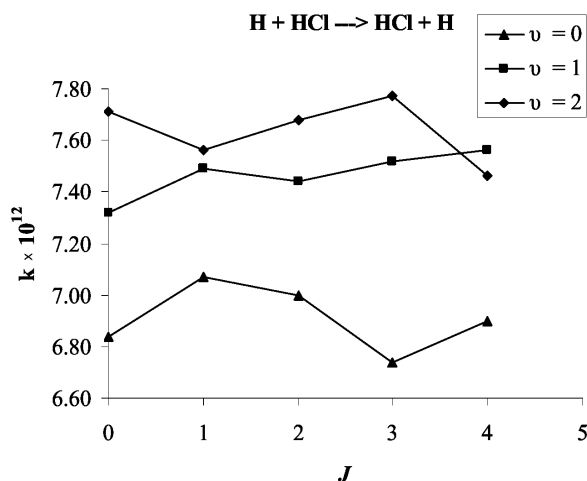


Fig. 17. Variation of the reaction rate constant  $k$  for the reaction  $\text{H} + \text{HCl} \rightarrow \text{HCl} + \text{H}$  with both  $\nu$  and  $J$  values.

molecules instead of the formation of  $\text{H}_2$  molecules. This is due to a deeper Morse potential well for  $\text{HCl}$  (5.32 eV) compared with that for  $\text{H}_2$  (5.08 eV). Yao et al. [28] performed a time-dependent wave packet calculation for the reaction  $\text{H} + \text{HCl}$  and its isotopic reac-

tions. The calculations were carried out on the potential energy surface (PES) of Bian and Werner (BW2). Reaction probabilities for the exchanged and abstraction channels were calculated from various initial rotational states of the reagent. For the  $\text{H} + \text{HCl}$  reaction, they found that, with an increase of  $J$ , the reaction probability *generally* decreases in the abstraction channel (formation of  $\text{H}_2$ ) and *generally* increases in the exchange channel (formation of  $\text{HCl}$ ). This is in agreement of our findings as shown in Figs. 14 and 16.

#### 4. Conclusions

Effects of the vibrational and rotational energy on the reaction probability, cross-section and rate constant for atom-diatomic molecule collisions have been studied in three dimensions using Monte Carlo classical trajectories. Morse potential energy surfaces were applied to describe the interactions between colliding adjacent particles. Various atoms and various diatomic molecules were selected in this study. In general, the results showed that the reaction cross-section (as well as probability and rate constant) increases as the vibrational quantum number of the molecule ( $\nu$ ) increases. However, for most systems studied, it was found that the rotational quantum number ( $J$ ) has a minor effect on the reaction cross-section. Results of calculations were compared among the systems studied and with available experimental values. Comparison had been also made with theoretical values obtained by other researchers using different potential energy surfaces and different calculation methods. Overall, good agreement was observed with the experiment and other calculated results. These findings should improve our understanding of the dynamical mechanism of reactions in the collision process. The classical trajectories method provides an *approximate* and simple way to predict rate constants for systems which, by nature, belong to the quantum mechanical world.

- [1] H. M. Abdel-Halim and S. M. Jaafreh, *Z. Naturforsch.* **63a**, 159 (2008).
- [2] R. N. Porter, M. Karplus, and R. D. Sharma, *J. Chem. Phys.* **43**, 3259 (1965).
- [3] A. Persky, *J. Chem. Phys.* **70**, 3910 (1979).
- [4] R. Schinke and W. A. Lester, *J. Chem. Phys.* **70**, 4893 (1979).
- [5] C. Zuhrt, F. Schneider, U. Havemann, L. Zulicke, and Z. Herman, *Chem. Phys.* **38**, 205 (1979).
- [6] J. C. Weisshaar, T. S. Zwier, and S. R. Leone, *J. Chem. Phys.* **75**, 4873 (1981).
- [7] D. L. Phillips, H. B. Levene, and J. J. Valentini, *J. Chem. Phys.* **90**, 1600 (1989).
- [8] F. J. Aoiz, V. Candela, V. J. Herrero, and V. S. Rabanos, *J. Chem. Phys.* **169**, 243 (1990).
- [9] F. J. Aoiz, V. J. Herrero, and V. S. Rabanos, *J. Chem. Phys.* **94**, 7991 (1991).

- [10] S. L. Meilke, D. W. Schwenke, and D. G. Truhlar, *J. Phys. Chem.* **99**, 16210 (1995).
- [11] K. Moribayashi and H. Nakamura, *J. Phys. Chem.* **99**, 15410 (1995).
- [12] A. J. McCaffery, K. Truhins, and T. W. J. Whiteley, *J. Phys. B: At. Mol. Opt. Phys.* **31**, 2023 (1998).
- [13] S. T. Lee and J. M. Farrar, *J. Chem. Phys.* **111**, 7348 (1999).
- [14] R. J. Marsh, A. J. McCaffery, and M. A. Osborne, *J. Phys. Chem. A* **107**, 9511 (2003).
- [15] W. H. Miller, *J. Phys. Chem. A* **105**, 2942 (2001).
- [16] R. D. Harrison and H. Ellis (Eds.), *Book of Data*, The Nuffield-Chelsea Curriculum Trust, Essex, England 1984, pp. 18–22.
- [17] K. P. Huber and G. Herzberg, *Molecular Spectra and Molecular Structures. IV. Constants of Diatomic Molecules*, Van Nostrand Reinhold, New York 1979.
- [18] <http://physics.nist.gov/cgi-bin/MolSpec/mole.pl>
- [19] D. L. Bunker, in: *Methods in Computational Physics: Classical Trajectory Methods*, Vol. 10, Academic Press, New York 1971, p. 287.
- [20] See for example: P. L. Houston, *Chemical Kinetics and Reaction Dynamics*, McGraw-Hill, New York 2001, Chapter 3.
- [21] H. M. Abdel-Halim and B. I. Al-Shihi, *Ind. J. Chem.* **35**, 366 (1996).
- [22] D. W. Setser, J. P. Sung, and R. J. Malins, *J. Phys. Chem.* **83**, 1007 (1979).
- [23] J. T. Muckerman and M. B. Faist, *J. Phys. Chem.* **83**, 79 (1979).
- [24] A. Persky, *J. Chem. Phys.* **66**, 2932 (1977).
- [25] I. B. Bykhalo, V. V. Filatov, E. B. Gordon, and A. P. Perminov, *Russ. Chem. Bull.* **43**, 1637 (1994).
- [26] K. Tamagake and D. W. Setser, *J. Phys. Chem.* **83**, 1000 (1979).
- [27] R. Sayos, J. Hernando, R. Francia, and M. Gonzalez, *Phys. Chem. Chem. Phys.* **2**, 523 (2000).
- [28] L. Yao, K. L. Han, H. S. Song, and D. H. Zhang, *J. Chin. Chem. Soc.* **50**, 565 (2003).